Proceedings of the 17th World Congress
The International Federation of Automatic Control
Seoul, Korea, July 6-11, 2008

Band-reconfigurable Multi-UAV-based Cooperative Remote Sensing for Real-time Water Management and Distributed Irrigation Control

Haiyang Chao * **Marc Baumann** ** **Austin Jensen** *
YangQuan Chen * **Yongcan Cao** * **Wei Ren** * **Mac McKee** ***

* *CSOIS, Electrical & Computer Engineering Department, Utah State University, Logan, USA 84322-4120*
** *Ravensburg-Weingarten University, Weingarten, Germany 88241*
*** *Utah Water Research Laboratory, Civil & Environment Engineering Department, Utah State University, Logan, USA 84322-4110*

Abstract: This paper presents an overview of ongoing research on small unmanned autonomous vehicles (UAVs) for cooperative remote sensing for real-time water management and irrigation control. Small UAVs can carry embedded cameras with different wavelength bands, which are low-cost but have high spatial-resolution. These imagers mounted on UAVs can form a camera array to perform multispectral imaging with reconfigurable bands dependent on mission. Development of essential subsystems, such as the UAV platforms, embedded multispectral imagers, and image stitching and registration, is introduced together with real UAV flight test results of one typical example mission.

Keywords: Unmanned aerial vehicle, low cost multispectral imaging, cooperative remote sensing, water management, irrigation control.

1. INTRODUCTION

Recently, there has been increasing interest in using small unmanned air vehicles (UAVs) for civilian applications [Chao et al., 2007b] such as in traffic control, border patrol, forest fire monitoring [Casbeer et al., 2005], agriculture mapping, etc. UAVs can save human pilots from dangerous and tedious jobs, reduce maintenance and operational costs and provide information more promptly and accurately than manned aircrafts or satellites. Moreover, with the developments of wireless technology and micro electromechanical systems, groups or even swarms of small UAVs can be employed for more challenging missions such as real-time large-scale system mapping and surveillance in the near future.

Water management and irrigation control are becoming more important due to the increasing scarcity of water across the world. However, it is difficult to sense and estimate the state of water systems because most water systems are large-scale and need monitoring of many factors including the quality, quantity, and location of water, soil and vegetations. For the mission of accurate sensing of a water system, ground probe stations are expensive to build and can only provide data with very limited sensing range. Satellite photos can cover a large area, but have a low resolution and a slow update rate. Small UAVs cost less money but can provide more accurate information from low altitudes with less interference from clouds. Small UAVs combined with ground and orbital sensors can even form a multi-scale remote sensing system.

UAVs equipped with imagers have been used in several agricultural remote sensing applications for collecting aerial images. High resolution red-green-blue (RGB) aerial photos can be used to determine the best harvest time of wine grapes [Johnson et al., 2003]. Multispectral images are also shown to be potentially useful for monitoring the ripeness of coffee [Johnson et al., 2004]. Water management is still a new area for UAVs, but it has more exact requirements than other remote sensing applications: real-time management of water systems requires more and more precise information on water, soil and plant conditions, for example, than most surveillance applications. Most current UAV remote sensing applications use large and expensive UAVs with heavy cameras and collect only one band of aerial imagery. Images from reconfigurable bands taken simultaneously can increase the final information content of the imagery and significantly improve the flexibility of the remote sensing process. Furthermore, less effort might be required for the georeferencing problem (i.e., stitching the UAV images into a useful composite image).

Motivated by the above water resources problem, a band-configurable, small UAV-based remote sensing system has been developed in steps. The objective of this paper is to present an overview of the ongoing research on this topic.

This paper is organized as follows. The remote sensing requirements for water management and irrigation control are discussed in Sec. 2. Based on this, a band reconfigurable small UAV remote sensing system is proposed in Sec. 3. Then, coverage control of a single UAV and multiple UAVs with certain imagers is explained in detail. Subsystem development of components such as UAV platform, embedded multispectral imager, image stitching and georeference capabilities are introduced in Sec. 4. Finally real field flight test results are shown in Sec. 5.

2. WATER MANAGEMENT AND IRRIGATION CONTROL REQUIREMENTS

The goal of irrigation control is to minimize the water consumption while sustaining the agriculture production and human needs [Fedro et al., 1993]. This optimiza-

⋆ Corresponding authors: Profs. YangQuan Chen and Wei Ren. Emails: yqchen@ieee.org and wren@engineering.usu.edu

tion problem requires remote sensing to provide real-time (daily or weekly) feedback from the field including:

- Water: water quantity and quality with temporal and spatial information, for example water level of a canal.
- Soil: soil moisture and type with temporal and spatial information.
- Vegetation: vegetation index, quantity and quality with temporal and spatial information, for example the stage of growth of the crop.

2.1 Introduction to Multispectral Remote Sensing

The purpose of remote sensing is to acquire information about the Earth's surface without coming into contact with it. One objective of remote sensing is to characterize the electromagnetic radiation emitted by objects [James, 2006]. Typical divisions of the electromagnetic spectrum include the visible light band ($380-720nm$), near infrared (NIR) band ($0.72-1.30\mu m$), and mid-infrared (MIR) band ($1.30-3.00\mu m$). Band-reconfigurable imagers can generate several images from different bands ranging from visible spectra to infra-red or thermal based for various applications. The advantage of the ability to examine different bands is that different combinations of spectral bands can have different purposes. For example, the combination of red-infrared can be used to detect vegetation and camouflage [Johnson et al., 2004].

2.2 Problem Statement of Remote Sensing

Let $\Omega \subset R^2$ be a polytope including the interior, which can be either convex or nonconvex. A series of band density functions $\eta_{rgb}, \eta_{nir}, \eta_{mir} \ldots$ are defined as $\eta_i(q,t) \in [0,\infty)$ $\forall q \in \Omega$. η_{rgb} can also be treated as three bands η_r, η_g, η_b, which represent RED, GREEN and BLUE band values of a pixel. The goal of remote sensing is to make a mapping from Ω to $\eta_1, \eta_2, \eta_3 \ldots$ with a preset spatial and temporal resolution for any $q \in \Omega$ and any $t \in [t_1, t_2]$.

A ground-based sensing device can provide a highly accurate mapping but with a limited range (inch level spatial resolution and second level temporal resolution). Satellite photos can provide global level resolution with a large range (about 30-250 meter or lower spatial resolution and week level temporal resolution). But these photos are expensive and cannot be updated at the desirable spatial or temporal scales. UAVs can provide a high resolution (meter or centimeter spatial resolution and hour-level temporal resolution) even with an inexpensive camera since satellites can not fly so low as small UAVs.

3. REMOTE SENSING USING SMALL UAVS

Small UAVs are UAVs that can be operated by only one or two people with a flight height less than 10,000 feet above the ground surface. Many of them can be hand-carried and hand-launched. Small UAVs with cameras can easily achieve a meter-level spatial resolution because of their low flight elevations. However, this also leads to a smaller footprint size which represents a limitation on the area that each image can cover. In other words, more georeferencing work is needed to stitch or put images taken at different places together to cover a large-scale water system. Thus the UAV remote sensing mission can be divided into two subproblems:

- Coverage control problem: path planning of the UAV to take aerial images of the whole Ω.
- Georeference problem: registry of each pixel from the aerial images with both temporal and spatial information, for example the GPS coordinates and time at which the picture was taken.

There can be two types of solutions. The open-loop solution is to solve the two subproblems separately with the coverage control problem before the UAV flight, and the georeference problem after it. This method is simple and easy to understand but requires significant experience to set up all the parameters. The close-loop solution is to do the path planning and georeference in real-time so that the information from the georeference part can be used as the observer for the path planning controller. This paper focuses on an open-loop solution.

3.1 Coverage Control

Coverage Control Subproblem

Given a random area Ω, UAVs with functions of altitude and speed maintenance and waypoint navigation: speed $v \in [v_1, v_2]$, possible flight height $h \in [h_1, h_2]$, camera with specification: focal length F, image sensor pixel size: $PS_h \times PS_v$, image sensor pixel pitch $PP_h \times PP_v$, the interval between images acquired by the camera (the "camera shooting interval") t_{shoot}, the minimal shooting time $t_{shoot_{min}}$, the desired aerial image resolution res, the control objective is:

$$\min t_{flight} = g(\Omega, h, v, \{q_1, \ldots, q_i\}, t_{shoot}, res), \qquad (1)$$

$s.t. v \in [v_1, v_2], h \in [h_1, h_2], t_{shoot} = k \times t_{shoot_{min}}$. where t_{flight} is the flight time of the UAV for effective coverage, $g(\Omega, h, v, t_{shoot})$ is the function to determine the flight path and flight time for effective coverage, k is a positive integer.

The control inputs of the coverage controller include bounded velocity v, bounded flight height H, a set of preset UAV waypoints $\{q_1, q_2, \ldots, q_i\}$ and the camera shooting interval t_{shoot}. The system states are the real UAV trajectory $\{\bar{q}_{t_1}, \ldots, \bar{q}_{t_2}\}$ and the system output is a series of aerial images or a video stream taken between t_1 and t_2.

Assume the imager is mounted with its lens vertically pointing down towards the earth, we use an approximation here; its footprint (shown in Fig. 1) can be calculated as:

$$FP_h = \frac{h \times PP_h \times PS_h}{F}, FP_v = \frac{h \times PP_v \times PS_v}{F}.$$

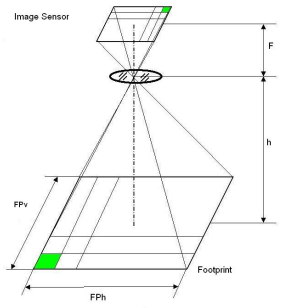

Fig. 1. Footprint Calculation.

Most UAVs can maintain altitude while taking pictures so the UAV flight height h can be determined first based on camera and resolution requirements. Assuming different flight altitudes have no effect on the flight speed, we get

$$h = \frac{\sqrt{res} \times F}{max(PP_h, PP_v)}. \qquad (2)$$

Given the flight height h and the area of interest Ω, the flight path, cruise speed and camera shooting interval

must also be determined. Without loss of generality, Ω is assumed to be a rectangular since most other polygons can be approximated by several smaller rectangles. The most intuitive flight path for UAV flight obtained by dividing the area into strips based on the group spatial resolution, shown in Fig. 2(a). The images taken during UAV turning are not usable because they may have bad resolutions. Due to the limitation from the UAV autopilot, GPS accuracy and wind, the UAV cannot fly perfectly straight along the preset waypoints. To compensate the overlapping percentage between two adjacent sweeps o must also be determined before flight; this compensation is based on experience from the later image stitching as shown in Fig. 2(b).

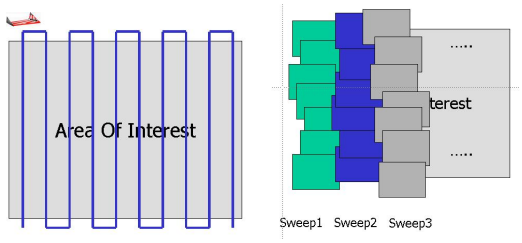

(a) Ideal Trajectory (b) Real Trajectory

Fig. 2. UAV Flight Path.

Given the overlapping percentage $o\%$ between sweeps, the ground overlapping o_g can be determined by:

$$o_g = (1 - o\%) \times FP_h. \tag{3}$$

The minimal camera shooting interval is computed as:

$$t_{shoot_{min}} = \frac{(1 - o\%) \times FP_v}{v}. \tag{4}$$

This open-loop solution is intuitive, robust to all the polygons and requires little computation. However, this method requires that many parameters, especially the overlapping percentage $o\%$ to be set up based on experience; it cannot provide an optimal solution. More work on a close-loop real-time solution is needed for an optimal solution.

3.2 Georeference Problem

After the aerial images are taken and sent back to the ground, post flight image processing is needed since the UAV cannot maintain perfectly level flight all the time especially during turning [Randy and Sirisha, 2005, Xiang and Tian, 2007, Sridhar et al., 2007].

Problem Statement for Post Flight Image Stitching

Given the aerial images stream $\{I_1, I_2, \ldots, I_m\}$ and the UAV flight data logger stream $\{t_1, t_2, \ldots, t_n\}$, $\{q_1, q_2, \ldots, q_n\}$ $\{\psi_1, \psi_2, \ldots, \psi_n\}$, $\{\theta_1, \theta_2, \ldots, \theta_n\}$, $\{\phi_1, \phi_2, \ldots, \phi_n\}$, map $\eta(R^3, \psi, \theta, \phi, t)$ back to $\eta(R^2, 0, 0, \phi, t)$, where ψ, θ and ϕ represent the roll, pitch and yaw angles respectively.

This problem can be solved by feature based mapping, or geology information based mapping, or both.

Feature Based Stitching With feature based stitching, the aerial images are stitched together based on some common features such as points, lines or corners. These features can either be specified manually by humans or recognized automatically by some algorithms. For example, PTGUI software needs reference points to perform image stitching. This method works well for photos sharing several common features. A simple example is shown in Fig. 3. The aerial photos were taken at about 150 meters above the ground by a GF-DC (introduced in Sec. 4) mounted on a model airplane controlled by a human operator. The problem with this method is that the photos are not georeferenced, and with no absolute coordinates to tie to, the error can keep increasing with the image numbers. Because of the small image footprint of small UAVs and the lack of permanent distinguishing features of most agricultural fields, it is almost impossible to find enough common features in every picture to correctly tie the photos together. There are also feature-based stitching methods that georeference the photos. These take features on each photo and compare them to photos which already have GIS information. This method performs the stitching task better because each photo is georeferenced and has some absolute coordinates to tie to. However, the photos with the GIS information are often taken once a year. For some photos taken from the UAV, they are not current enough to find similar features.

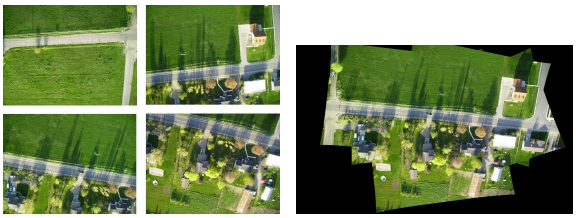

(a) Photos before Stitch (b) Photos after Stich

Fig. 3. Feature Based Stiching.

UAV Position and Attitude Based Stitching This method uses the data from the UAV including R^3, θ, ϕ, ψ to map the image back to the related ground frame and registry each pixel with its ground coordinates and electromagnetic density values. The advantage is that this method uses the information from the UAV and can guarantee a bounded global error even for the final big image. However, it requires perfect synchronization between the aerial images and the UAV attitude logging data, which means the full authority in UAV autopilot and sensor package. It is one of the disadvantages of using off-the-shelf UAVs for remote sensing missions.

The related reference frames for UAV remote sensing are defined as follows, shown in Fig. 4(a):

(1) Camera Frame: F_{cam}, the reference frame with the origin at the focal point and the axes as shown in Fig. 4(b).
(2) UAV Body Frame: F_{body}, the reference frame with the origin at the UAV center and the axes pointing forward, right and down.
(3) Navigation Frame: F_{nav}, the reference frame with a specific ground origin and the axes pointing the North, East and down to the Earth center.
(4) GPS Frame: F_{GPS}, the reference frame used by GPS. It has a format of Latitude, Longitude and Altitude.

A three-dimensional (3D) mesh M_{hw} needs first be generated in F_{cam}, which describes the spatial distribution of its corresponding image. This mesh has $n \times n$ elements, illustrated in Fig. 4(b). Each element of (M_{hw}) can be calculated as:

$$q(w,h)_{cam} = \begin{bmatrix} x(w,h)_{cam} \\ y(w,h)_{cam} \\ f \end{bmatrix}, \forall q(w,h)_{cam} \in M_{wh}, \tag{5}$$

$$x(w,h)_{cam} = \frac{S_w(2w-n)}{2n}, y(w,h)_{cam} = \frac{S_h(2h-n)}{2n},$$

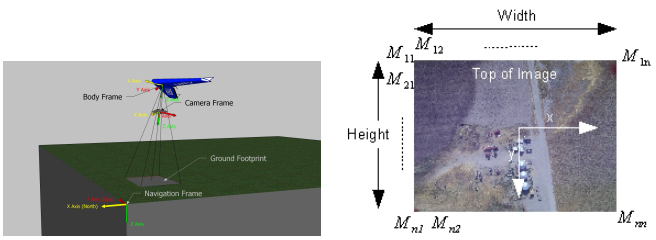

(a) Coordinates (b) Camera Frame & Mesh

Fig. 4. Definition of Coordinates & Meshes.

where $w, h \in [1, n]$, f is the focal length of the camera, w is the column index of the mesh, h is the row index of the mesh, S_w and S_h are the width and height of the image sensor respectively.

The mesh needs to be rotated first with respect to F_{body}, F_{nav} and then translated to the ground frame F_{gps}. The manner in which the camera is mounted on the UAV body decides the rotation matrix R^{cam}_{body}, which can be a constant or a dynamic matrix. For example, a gimballed camera that can rotate. The angles (yaw, pitch and roll ψ_c, θ_c, ϕ_c) describe the orientation of the camera with respect to the body.

$$R^{cam}_{body} = (R^{body}_{cam})^T = (R_{zyx}(\psi_c + 90, \theta_c, \phi_c))^T, \quad R^{cam}_{body}, R^{body}_{cam} \in SO(3). \tag{6}$$

The rotation matrix from F_{body} to F_{nav} can be determined from the orientation of the aircraft (ψ, θ, ϕ) with respect to the navigation coordinate system, which can be measured by the UAV onboard sensors.

$$R^{body}_{nav} = \begin{bmatrix} c_\theta c_\psi & -c_\phi s_\psi + s_\phi s_\theta c_\psi & s_\phi s_\psi + c_\phi s_\theta c_\psi \\ c_\theta s_\psi & c_\phi c_\psi + c_\phi s_\theta s_\psi & -s_\phi c_\psi + c_\phi s_\theta s_\psi \\ -s_\theta & s_\phi c_\theta & c_\phi c_\theta \end{bmatrix}, \quad R^{body}_{nav} \in SO(3), \tag{7}$$

where c_θ, s_θ stand for $cos(\theta)$ and $sin(\theta)$ respectively and similarly for the other terms.

The rotation transformations can be then calculated with all the above rotation matrices:

$$q_{nav} = R^{body}_{nav} \quad R^{cam}_{body} \quad q_{cam}, \tag{8}$$

The mesh now represents the location of the image sensor in the Navigation Frame F_{nav}. To represent the location of the picture on the earth, the vectors in the mesh are scaled down to the ground. It is assumed that the earth is flat because each picture has such a small footprint. q_{nav} is the element of the new projected mesh, $q_{nav}(z)$ is the z component of the element in the unprojected mesh, and h is the height of the UAV when the picture was taken.

$$q^P_{nav} = \frac{h}{q_{nav}(z)} q_{nav}. \tag{9}$$

The elements of the mesh are now rotated into ECEF coordinates using the latitude (λ) and the longitude (φ) of the UAV when the picture was taken. Then the mesh is translated by the position vector $(\overrightarrow{P})$ of the UAV in ECEF coordinates.

$$R^{nav}_{gps} = R_{yyz}(-\lambda, 90^\circ, \varphi), \qquad R^{nav}_{gps} \in SO(3), \tag{10}$$

$$q_{gps} = R^{nav}_{body} \quad q^P_{nav} + \overrightarrow{P}, \tag{11}$$

After the above calculations, the meshes can be further processed by some 3-D imaging software like World Wind [NASA, 2007]. World Wind can place the meshes correctly on the earth and provide an interactive 3-D displaying. More details are shown in Sec. 4.

3.3 Multi-UAV Approach

Some irrigation applications may require remote sensing of a large land area (more than 30 square miles) within a short time (less than one hour). Acquisition of imagery on this geographic scale is difficult for a single UAV. However, groups of UAVs (which we call "covens") can solve this problem because they can provide images from more spectral bands in a shorter time than a single UAV.

The following missions will need multiple UAVs (covens) operating cooperatively for remote sensing:

- Measure $\eta_1, \eta_2, \eta_3 \ldots$ simultaneously.
- Measure $\eta_i(q, t)$ within a short time.

To fulfill the above requirements, UAVs equipped with imagers having different wavelength bands must fly in some formation to acquire the largest number of images simultaneously. The reason for this requirement is that electromagnetic radiation may change significantly, even over a period of minutes, which in turn may affect the final product of remote sensing. The "V" or "—" formation keeping algorithm, similar to the axial alignment [Ren et al., 2008], can be used here since the only difference is that the axis is moving:

$$\dot{q}^d_m = - \sum_{n \in \mathcal{J}_m(t)} [(q_m - q_n) - (\delta_m - \delta_n)], \tag{12}$$

where q^d_m is the preset desired waypoints, $\mathcal{J}_m(t)$ represents the UAV group, $\delta_m = [\delta_{mx}, \delta_{my}]^T$ can be chosen to guarantee that the UAVs align on a horizontal line with a certain distance in between.

4. SUBSYSTEMS DEVELOPMENT

To achieve the final goal of measuring the density functions of different bands simultaneously, subsystems have been purchased, upgraded or developed separately including the UAV platform subsystem, embedded imager subsystem and image processing subsystem.

4.1 UAV Platform

Three types of different UAV platforms are undergoing testing in the Center for Self Organizing and Intelligent Systems (CSOIS) including off-the-shelf Procerus UAV, Xbow UAV with open source software and Parparrazi UAV with both open source software and open source hardware. For details, see [Chao et al., 2007a, Baumann, 2007].

4.2 Embedded Imager Development [Baumann, 2007]

The weight, shape of the imager, and manner in which the imager is mounted can significantly affect UAV flight dynamics. Due to the physical limitations of a small UAV platform, the embedded imager must be small, light and consume low power. For example, the Procerus 48" UAV can only carry extra payload of less than one pound. Four types of embedded imagers have been developed for small UAV applications: ghost finger RGB/NIR digital camera (GF-RGB/NIR-DC), ghost finger RGB/NIR digital video camera (GF-RGB/NIR-DV).

Ghost Finger Digital Camera (GF-DC) The "ghost finger digital camera" (GF-DC) is developed from a Pentax OPTIO E30 digital camera. Three photo capturing modes are included: timer triggered, remote control (RC) triggered, and digital switch triggered. An ATMEG8L microcontroller is embedded with the camera to serve as a camera trigger controller. The timer trigger shot mode is for aerial photo capturing with a preset shooting interval t_{shoot}. The RC triggered mode is to use spare channel from RC transmitter and receiver to control the picture capture. The switch triggered shot mode is for triggering from the UAV autopilot to achieve a better geospatial synchronization. The camera GF-DC is shown in Fig. 5. The images are saved on the SD card within the camera. The GF-DC has been tested to work for more than one hour in timer triggered mode with one 1GB SD card and a 3.7 V Li-poly battery (950mA-hour).

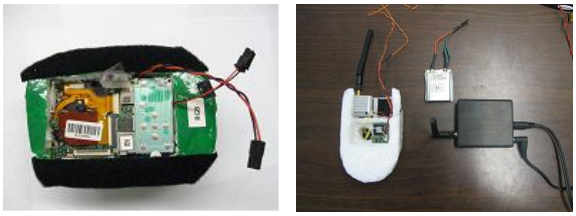

(a) GF-DC (b) GF-DV

Fig. 5. Ghost Finger Embedded Imager.

Ghost Finger Digital Video Camera (GF-DV) GF-DV is developed for real-time image transmission. It is comprised of a single board analog 1/4" CCD camera, one $2.4GHz$ black widow wireless video transmitter, and peripheral circuits. The CCD camera only weighs about 7.09g. The GF-DV is shown in Fig. 5(b). The communication range for the wireless transmitter and receiver can be up to one mile with the 3 dB antenna. The GF-DV requires a wireless video receiver to get the video back in real time and the video stream can be saved in an MPEG file.

RGB+NIR Imager Array Most CCD chips used on cameras are only sensitive to the electromagnetic light with a spectral wavelength ranging from 400 to 1100 nm, which includes both the visible and NIR bands. Digital cameras use an IR blocking filter to block wavelengths above $750nm$. A CCD-based camera can be changed into a NIR sensor by removing the IR blocking filter and adding one visual band blocking filter. A Lee 87 NIR filter is used in our GF-DC and GF-DV to block the light with the wavelength smaller than $730nm$. So, the Ghost Finger NIR imager has a band of about $730 - 1100nm$. The NIR filter is added on both GF-DC and GF-DV to form an array of two imagers, which can measure the RGB and NIR simultaneously. Sample RGB and NIR photos taken by GF-DC2 $\times$ 1 are shown in Fig. 6.

(a) RGB Photo (b) NIR Photo

Fig. 6. Sample Photos by GF-DC 2×1.

5. PRELIMINARY EXPERIMENTAL RESULTS

Preliminary experimental results are shown in this section to demonstrate the effectiveness of the whole UAV remote sensing system on both the hardware and software levels. One typical sample application is introduced in detail on acquisition of photographic data over Desert Lake, Utah. More experiment results can be found in CSOIS report [Chao et al., 2007a].

Desert Lake in west-central Utah (latitude: $39°22'5''N$, longitude: $110°46'52''W$) is formed from return flows from irrigated farms in that area. It is also a waterfowl management area. This proposes a potential problem because the irrigation return flows can cause the lake to have high concentrations of mineral salts, which can affect the waterfowls that utilize the lake. Managers of the Desert Lake resource are interested in the affect of salinity control measures that have been recently constructed by irrigators in the area. This requires estimation of evaporation rates from the Desert Lake area, including differential rates from open water, wetland areas, and dry areas. Estimation of these rates requires data on areas of open water, wetland, and dry lands, which, due to the relatively small size and complicated geometry of the ponds and wetlands of Desert Lake, are not available from satellite images. A UAV can provide a better solution for the problem of acquiring periodic information about areas of open water, etc., since it can be flown more frequently and at less cost.

5.1 Mission Description & Path Planning

The whole Desert Lake area is about 2×2 miles. It is comprised of four ponds and some wetland areas. The flight path must cover both the open water and wetland areas.

GFDV 2×1 is mounted in the middle of the Procerus UAV, and the lens is pointed vertically downwards to provide real-time, simultaneous RGB and NIR videos. Maxtream 900MHz modems are used for the UAV and ground station communication, and a 20 dB ground antenna is added to guarantee a communication range of 3 miles. The UAV flight parameters are computed before flight based on prior flight experience.

The flight height is computed as $H < 400m$ because submeter pixel resolution is enough for this application. Due to the safety issue and FMA regulations, the flight height is set to 200 meters. The flight path is planned based on the calculated parameters: flight height 200m, cruise speed 14 m/s, sweep overlap 270 m, camera sampling interval 5 seconds. The flight trajectory is shown in Fig 7.

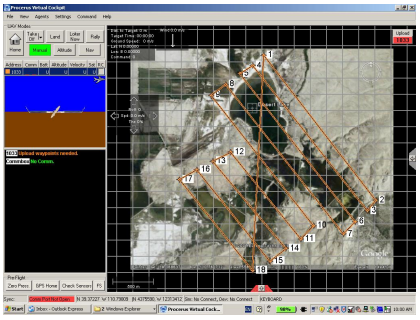

Fig. 7. UAV Preplanned Flight Path for Desert Lake Mission.

5.2 Experimental Result

Both the RGB and NIR videos are transmitted back to the ground station in real time and saved on the base

laptop as a MPEG file for further processing. A time stamp with each photo is compared with the data log of the UAV to georeference each photo. Then the photos are viewed on an open source 3D interactive world viewer called World Wind [NASA, 2007]. A customer-built UAV plug-in combined with World Wind allows us to place each picture on the globe to see how well the georeferencing is accomplished. Currently the plug-in takes the photos with the information from the UAV and displays them all on the globe to check how well the aerial photos match. Future plans are to improve stitching by blending the overlapping photos together. Fig. 8 shows about 120 pictures which have gone through this process and been displayed on World Wind.

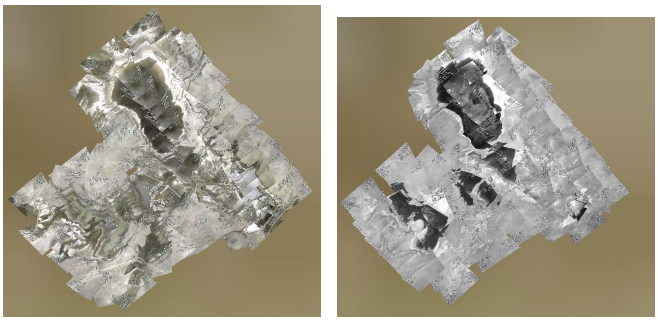

(a) RGB Band Aerial Photo (b) NIR Band Aerial Photo

Fig. 8. Photos after Stitch with GF-DV.

However, this application also shows some problems left unsolved including:

- Synchronization: The Procerus UAV sends the UAV data down to the base station and it is recorded on the computer at 1 to 3Hz depending on the communication. At the same time, our frame grabber grabs the pictures at 15 to 30 fps. The problem is that the picture may not match up perfectly with the UAV data on the data log. The picture may have been taken in between the data samples and may have an error up to 333ms. Methods for better synchronization are currently being developed and may show better results.
- Calibration: it is difficult to make a direct calibration for the aerial image and further stitching since the UAV usually needs to investigate a large area.
- Band configurable ability: the current platform only includes the RGB band and NIR bands, further more bands need to be added.
- Further image processing: the exact boundary of the lake needs to be decided combined with satellite images after applying advanced filtering techniques. Also, the current software requires manual post processing. For the application to be attractive to managers of real irrigation systems, manual post processing is unacceptable.
- Multiple UAVs: preliminary results have shown that the sensing range of the Procerus UAV with GFDV2 is about 2.5×2.5 miles, given the current battery energy density. However, light reflection varies a lot in one day and accurate NIR images require at most a two-hour acquisition time for capture of the entire composite image. This motivates the use of covens, or multiple UAVs, for this type of application, with each UAV carrying one imager with a certain bands.

6. CONCLUSION

This paper characterizes the problem of using UAVs for remote sensing in water management and irrigation control applications, and provides an outline of a band reconfigurable and multiple UAV solution to the problem. The big structure of the whole system, including both the hardware and software, are explained in detail. The preliminary results show the effectiveness of the proposed solution. More work on multi-spectral imagers and multi-UAV applications will be done.

ACKNOWLEDGEMENTS

This work is supported in part by the Utah Water Research Laboratory (UWRL) MLF Seed Grant (2006-2007) on "Development of Inexpensive UAV Capability for High-Resolution Remote Sensing of Land Surface Hydrologic Processes: Evapotranspiration and Soil Moisture." The authors would also like to thank Professor Raymond L. Cartee for providing the USU farm at Cache Junction as the flight test field, Dr. Roger Hansen and his staffs of the Bureau of Reclamation's Provo Area office, US Department of Interior for many stimulating meetings and discussions.

Haiyang Chao and Yongcan Cao were partly supported by Utah State University Vice President of Research Fellowship.

REFERENCES

Marc Baumann. Imager development and image processing for small UAV-based real-time multispectral remote sensing. Master's thesis, University of Applied Sciences Ravensburg-Weingarten and Utah State University, Weingarten, Germany and Logan, Utah, October 2007.

D. W. Casbeer, S. M. Li, R. W. Beard, T. W. McLain, and R. K. Mehra. Forest fire monitoring with multiple small UAVs. *Proceedings of the American Control Conference*, 5:3530–3535, June 2005.

H. Y. Chao, M. Baumann, A. M. Jensen, Y. Q. Chen, Y. C. Cao, W. Ren, and M. McKee. Band-reconfigurable multi-UAV-based cooperative remote sensing for real-time water management and distributed irrigation control. CSOIS Internal Technical Report USU-CSOIS-TR-07-02, Utah State University, 2007a.

H. Y. Chao, Y. C. Cao, and Y. Q. Chen. Autopilots for small fixed wing unmanned air vehicles: a survey. *Proceedings of IEEE International Conference on Mechatronics and Automation*, pages 3144–3149, August 2007b.

S. Zazueta Fedro, G. Smajstrla Allen, and A. Clark Gary. Irrigation system controllers. *Series of the Agricultural and Biological Engineering Department, Florida Cooperative Extension Service, Institute of Food and Agricultural Sciences, University of Florida*, 1993. URL `http://edis.ifas.ufl.edu/AE077`.

B. C. James. In *Introduction to Remote Sensing*, pages 28–52. Guilford Press, 4th edition, 2006.

L. F. Johnson, S. R. Herwitz, S. E. Dunagan, B. M. Lobitz, D. V. Sullivan, and R. E. Slye. Collection of ultra high spatial and spectral resolution image data over california vineyards with a small UAV. *Proceedings of the 30th International Symposium on Remote Sensing of Environment*, 2003.

L. F. Johnson, S. R. Herwitz, B. M. Lobitz, and S. E. Dunagan. Feasibility of monitoring coffee field ripeness with airborne multispectral imagery. *Applied Engineering in Agriculture*, 20:845–849, 2004.

NASA. World Wind software. 2007. URL `http://worldwind.arc.nasa.gov/index.html`.

R. P. Randy and P. Sirisha. Development of software to rapidly analyze aerial images. *American Society of Agricultural and Biological Engineers Annual International Meeting*, 2005.

W. Ren, H. Y. Chao, W. Bourgeous, N. Sorensen, and Y. Q. Chen. Experimental validation of consensus algorithms for multi-vehicle cooperative control. *IEEE Transactions on Control Systems Technology*, to appear 2008.

S. M. Sridhar, C. C. Collins, G. D. Chandler, M. T. Smith, and J. E. Lumpp. CATOPS: A composite aerial terrain orthorectification photography system for unmanned aircraft. *AIAA Infotech@Aerospace 2007 Conference and Exhibit*, May 2007.

H. Xiang and L. Tian. Autonomous aerial image georeferencing for a UAV based data collection platform using integrated navigation system. *American Society of Agricultural and Biological Engineers Annual International Meeting*, 2007.